Comparison of lidar and transmissometer measurements through clouds

Luc R. Bissonnette

DREV-Defence Research Establishment Valcartier
Mailing address: P.O. Box 8800, Courcelette, Québec, Canada , G0A 1R0
Street address: 2459, Pie XI Blvd. North, Courcelette, Québec, Canada, G0A 1R0
Tel.: +418-844-4437 • *Fax*: +418-844-4511 • *E-mail*: lbisson@asterix.drev.dnd.ca

Gerard Kunz

TNO Physics and Electronics Laboratory
Mailing address: P. O. Box 96864, The Hague, The Netherlands
Street address: 2509 JG The Hague, The Netherlands
Tel.: +31 70 374 0460 • *Fax*: +31 70 328 0961 • *E-mail*: kunz@fel.tno.nl

Karin Weiss-Wrana

Forschunginstitut für Optik (FfO)
Mailing and street address: Schloss Kressbach, D-72072 Tübingen, Germany
Tel.: +49 7071 709 177 • *Fax*: +49 7071 709 270 • *E-mail*: ioam@ipserv.ffo.fgan.de

ABSTRACT

A lidar-transmissometer intercomparison was made during an international experiment held in the German Alps to characterize the vertical structure of aerosols and clouds. The transmission path was 2325-m long and inclined at 30° along the slope of a steep mountain ridge. The transmissometer consisted of a Nd:YAG and a CO_2 laser located in the valley and a large-mirror receiver that captured the full beams on the mountain top. Two lidars, one at 1.06 μm and one at 1.054 μm, were operated with their axes approximately parallel to the transmissometer axis but separated by a horizontal distance on the order of 20-40 m. The first one was operated in retroreflector mode and the relative transmittance was determined from the reflection off the mountain ridge above the cloud layer. The second one had a special receiver designed to make simultaneous recordings at four fields of view. The range-resolved scattering coefficient and effective cloud droplet radius are calculated from these four-field-of-view measurements by solving a simplified model (Appl. Opt. **34**, 6959-6975, 1995) of the multiply scattered returns. The two simultaneous solutions for the scattering coefficient and effective droplet size make possible extrapolation at wavelenghths other than the lidar wavelength of 1.054 μm. The main measurement event analyzed in this paper lasted 1.5 hours and produced transmittances ranging from less than 5% to more than 90%. The comparisons show good correlation between the transmissometer data and all lidar solutions including extrapolation at 10.59 μm.
Key words: Cloud transmittance, Laser transmissometer, Aerosol lidar, Multiple aerosol scattering, Lidar inversion

1 INTRODUCTION

Researchers have long been using lidars to detect and characterize atmospheric constituents and pollutants. The principal advantages are remote sensing, and the high spatial and temporal resolutions they can provide. However, lidars have achieved mixed success for aerosols in inhomogeneous media.

One difficulty is the inversion of the lidar measurements to solve for the aerosol properties. The problem is well known and has been documented in numerous papers, for example Refs. 1-14. Methods have been developed that give satisfactory results in many situations provided some additional information can be obtained. To avoid recourse to separate instrumentation, various groups have proposed modifications to the conventional lidar technique. Noteworthy approaches include the high-spectral-resolution[15,16], the Raman[17], and the multiple-scattering[18] lidars. The technical implementation is different in all cases but the objective is the same: derive more aerosol information from the lidar returns. All these efforts are pointing toward the development of practical and reliable inversion techniques for aerosol lidar measurements.

A second difficulty is the experimental validation of the proposed inversion methods. Properties of natural or man-made aerosols intrinsically fluctuate in both space and time. The lidar can follow these fluctuations with good spatial and temporal resolutions but no independent instrument can provide the necessary detailed data to verify the complete solutions. Even for limited comparison points, there remain the problems of achieving spatial and temporal coincidence and matching the resolution scales.

This paper reports on a joint effort at producing good-quality validation data by conducting simultaneous lidars and transmissometer measurements along parallel paths chosen as close to each other as possible. The experiment geometry was a 2325-m long, 30°-elevation slant path along a steep mountain slope. Clouds regularly formed and dissipated between the valley and the mountain top stations giving rise to inhomogeneous and variable transmission conditions. The paper discusses the results of comparisons made between the solutions derived from two different lidars, a conventional single-scattering and a multiple-scattering lidar, and the transmissometer data for a cloud dissipation event that saw the transmittance at 1.064 μm vary from less than 5% to more than 90%.

2 EXPERIMENT

The experiment was the result of a close cooperation within a NATO research study group. It took place at Oberjettenberg near Bad Reichenhall in the German Alps in October 1992. The main advantage of the site was the ready access to facilities for setting up a transmissometer between the valley and the mountain top and performing simultaneous lidar measurements alongside the transmissometer axis. The aerosols of interest were the cloud and haze layers that drifted at intermediate altitudes between the valley and the summit. They provided, even in a single event, the full range of extinction values that a lidar can probe.

2.1 Transmissometer

The FGAN Forschunginstitut für Optik (FfO), Tübingen, Germany, designed, constructed and operated a one-way laser transmissometer to measure the atmospheric transmittance at 1.064 μm and 10.59 μm over a slant path of 2325 m along the mountain slope very close to the optical axes of the lidar systems. The measured transmittance values correspond to values integrated over the whole inhomogeneous propagation path.

The transmitter was located in the valley at 632 m above sea level (ASL) and the receiver at the summit of the Wartsteinkopf peak at 1758 m ASL. Transmittance measurements were performed with two IR lasers: a
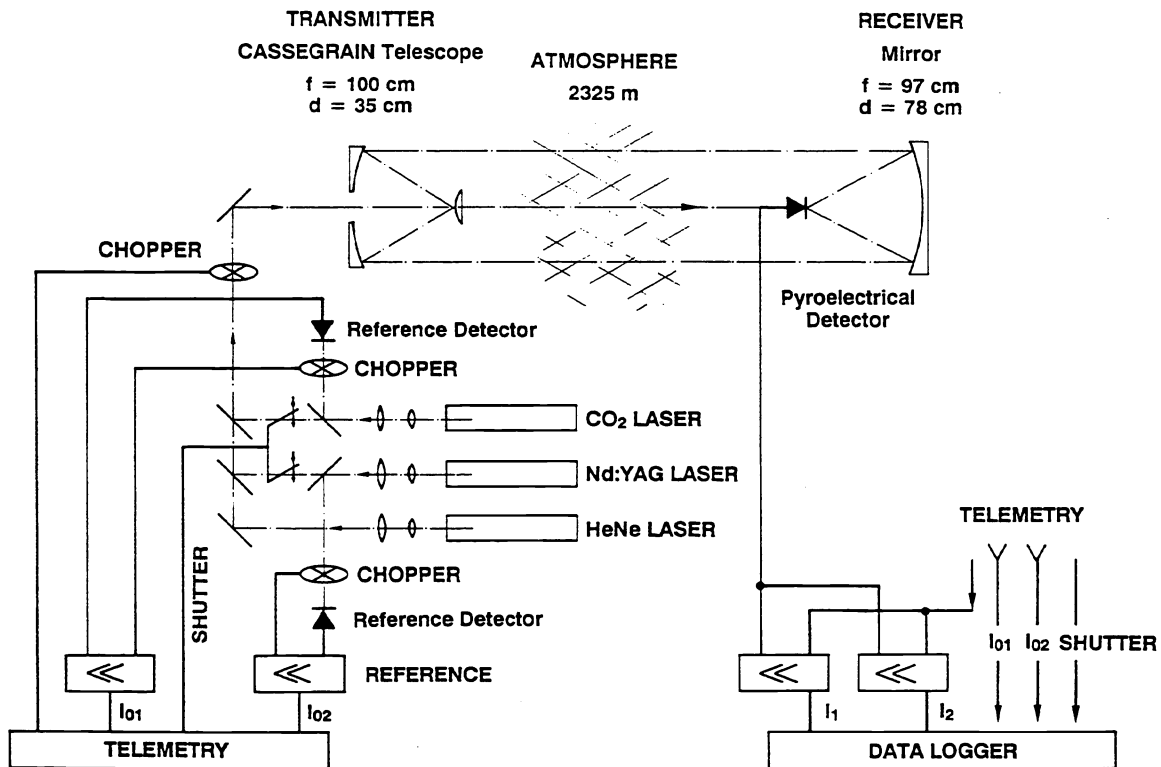
Figure 1: Block diagram of the laser transmissometer.

Nd:YAG laser at a wavelength of 1.064 μm and a CO_2 laser at a wavelength of 10.59 μm.

A block diagram of the transmissometer is shown in Fig. 1. The 350-mW cw Nd:YAG laser, the 3-W cw CO_2 laser and a HeNe laser at a wavelength of 0.633 μm, the latter used for alignment purposes only, were aligned coaxially by using appropriate dichroic beam splitters. Additional beam splitters reflected a low percentage of the IR power onto reference detectors to monitor the laser output power during the measurements. A Cassegrain telescope expanded the transmitted laser beams and focused them onto the receiver mirror which was large enough to capture the complete turbulence- and jitter-broadened laser beams. The receiver mirror focused the transmitted laser beam radiation onto a pyroelectrical detector.

Synchronous detection was employed for background rejection. The measurement frequency was set at 1 Hz. The two IR lasers were alternately turned off and on at intervals of 15 s. The reference signal of the shutter was used as a coding signal indicating which of the two lasers was being transmitted at a given time. This coding signal and the output signals of the reference detectors of both IR lasers were transmitted by radio link from the transmitter side to the receiver side and were acquired together with the sequential detector output signals for both lasers by a PC 12-bit computer and stored on a floppy disc.

The average value of the received laser power, $< Q >$, was calculated for series of 15 measurements at 1-s intervals, and used to determine the atmospheric transmittance τ. For a propagation path d, the transmittance

τ was calculated by the formula

$$\tau = \frac{<Q(d)>}{<Q(0)>}, \tag{1}$$

where $<Q(d)>$ is the average received power at distance d and $<Q(0)>$ is the average power at the transmitter aperture. $<(Q(0)>$ was determined by using the close-up calibration method in which the propagation range is reduced to zero $(d = 0)$ by bringing the receiver directly in front of the transmitter. The transmittance τ and the path-averaged extinction coefficient α are interrelated by Bouguers's law, i.e.

$$\tau = \exp(-\alpha d), \tag{2}$$

$$\alpha = -\frac{1}{d}\ln\tau. \tag{3}$$

The dynamic range of the laser transmissometer covered a broad range of extinction values. This was achieved by using interchangeable neutral density filters with appropriate attenuation factors. During the transmittance measurements, the sensitivity of the laser transmissometer could be adjusted to the changing meteorological conditions such as a dissipating cloud layer. The minimun detectable transmittance was $\sim 10^{-5}$, which corresponds to an average extinction coefficient α of ~ 5 km^{-1}. The relative errors in the measured transmittance, $\Delta\tau/\tau$, calculated by applying the error propagation law to the measured signal values, were found to be 6–7% in the case of the CO_2 laser radiation and 3–4% in the case of the Nd:YAG laser radiation.

2.2 SMAL lidar

At the TNO Physics and Electronics Laboratory, a Scanning Miniature Automatic Lidar (SMAL) has been designed, developed and constructed to rapidly scan a large volume and thus freeze the atmospheric dynamics as is required for cloud mapping purposes and for wind speed measurements[19]. The SMAL lidar uses a Nd:YAG laser, operating at a wavelength of 1.06 μm with a maximum repetition rate of ~ 13 Hz and a pulse energy of ~ 25 mJ. According to ANSI Z136.1-186[20], the nominal ocular hazard distance for a one-second exposure time is ~ 975 m and for an eight-hour exposure time is ~ 2650 m. The lidar receiver has an aperture area of 9.4×10^{-3} m^2 and a field of view of 2 mrad. The detector is an avalanche photo-diode with a temperature controlled bias; the minimum detectable optical power is ~ 5 nW in a 30-MHz electrical bandwidth. A second, synchronous lidar can be mounted on top of the main lidar for operation under a slightly different and adjustable azimuth angle. This mode is used for measuring the horizontal wind vector[21-22]. The receiver of this additional lidar was also used to measure the range-induced multiple scattering[23] that occurs off the laser beam axis. Logarithmic amplifiers are used to adapt the dynamic range of the signal to the 8-bit A/D converter. The 8-bit lidar waveforms are stored on optical disk and displayed on line in false color for monitoring and quality control purposes.

2.3 Multiple-Field-of-View (MFOV) lidar

The MFOV lidar is a lidar designed to measure the multiple scattering contributions to the aerosol backscatter signals. The MFOV hardware has already been described elsewhere[24-26]. The significant characteristics are summarized in Table 1. The source is a Nd:Glass laser normally operated at an energy of 1 J per pulse with a repetition frequency of 0.1 Hz. The optical receiver is a 150-mm diameter, f/1.33 refractive lens. It has a 0.4-mrad blur circle at ± 38 mrad off the receiver axis which provides good separation between the fields of view. The fields of view are defined by a four-element segmented photodiode array arranged as a circular central element surrounded by three ring-shaped elements and positioned in the focal plane of the receiver lens.

The laser source is mounted on top of the receiver and the beam is centered on the telescope axis by means of two 45° mirrors. The fields of view of the receiver are thus concentric with the laser beam. The central field of view is ~ 4 mrad full angle, i.e. one order of magnitude greater than the laser beam divergence. A smaller value

Lidar Source		Receiver	
Gain medium	Nd:Glass	Lens Diameter	152 mm
Wavelength	1.054 μm	Lens Focal Length	202 mm
Pulse Energy	1-2 J	Detector Type	p-i-n photodiode
Pulse Length (FWHM)	25 ns	Detector Response	0.35 A/W
Divergence	0.2 mrad	Detector Dark Current	$< 1 \mu$A at 80 V
Repetition rate	0.1 Hz	Detector Bias Voltage	80 V
		Detector Rise Time	< 25 ns
		1st Field of View	0 - 1.98 mrad
		2nd Field of View	2.30 - 6.39 mrad
		3rd Field of View	6.70 - 12.77 mrad
		4th Field of View	13.09 - 19.16 mrad
		Field of View Gap	0.32 ± 0.04 mrad

Table 1: MFOV Lidar Data

would have given a better discrimination of the single scattering contributions. However, this value was chosen because the first laser used had a divergence near 4 mrad and, in some experiments, the divergence of the current laser must be increased to meet eyesafety criteria at closer ranges.

The lidar was installed near the transmitter station of the transmissometer and was pointed about 15 mrad above the receiver station on the mountain peak. The misalignment was necessary for eyesafety reasons and for avoiding interference with the transmissometer operation. The separation between the lidar and transmissometer axes varied from about 15 m in the valley to about 35 m at the top of the mountain.

The MFOV lidar is a technique designed to retrieve the information contained in the multiple scattering contributions to lidar returns. It is described in Ref. [18]. The multiple scattering contributions are measured in the form of the field-of-view dependence of the lidar returns. At each range z, the signals measured in the four field-of-view channels are matched to a simple analytical model of the multiply scattered lidar return. This results in the determination, at each range z, of two aerosol properties: the scattering coefficient α_s at the lidar wavelength and the effective radius r_e of the aerosol particles. The solutions do not require the specification of a boundary value. A minimun of three fields of view is necessary to implement the inversion. From the α_s- and r_e-solutions and the assumption of a general form of the particle size distribution, for example a gamma function for the fog and cloud conditions of interest here, we can calculate the numerical values of the parameters of the assumed function and thus determine the droplet size distribution at every range z.

3   COMPARISON RESULTS

3.1   Transmissometer measurements

Figure 2 shows the diurnal variation of the transmittance measured on October 13 for both wavelengths of the laser transmissometer. The measurements started at 9h45 when a cloud layer with strong temporal and spatial variations was hanging at an altitude of about 900 m ASL while the summit of the mountain was in a clear cloudless atmosphere. The cloud gave rise to rapid fluctuations of the transmittance. The transmittance for the CO_2 laser radiation, $\tau(CO_2)$, is significantly higher than for the Nd:YAG laser radiation, $\tau(YAG)$; $\tau(CO_2)$
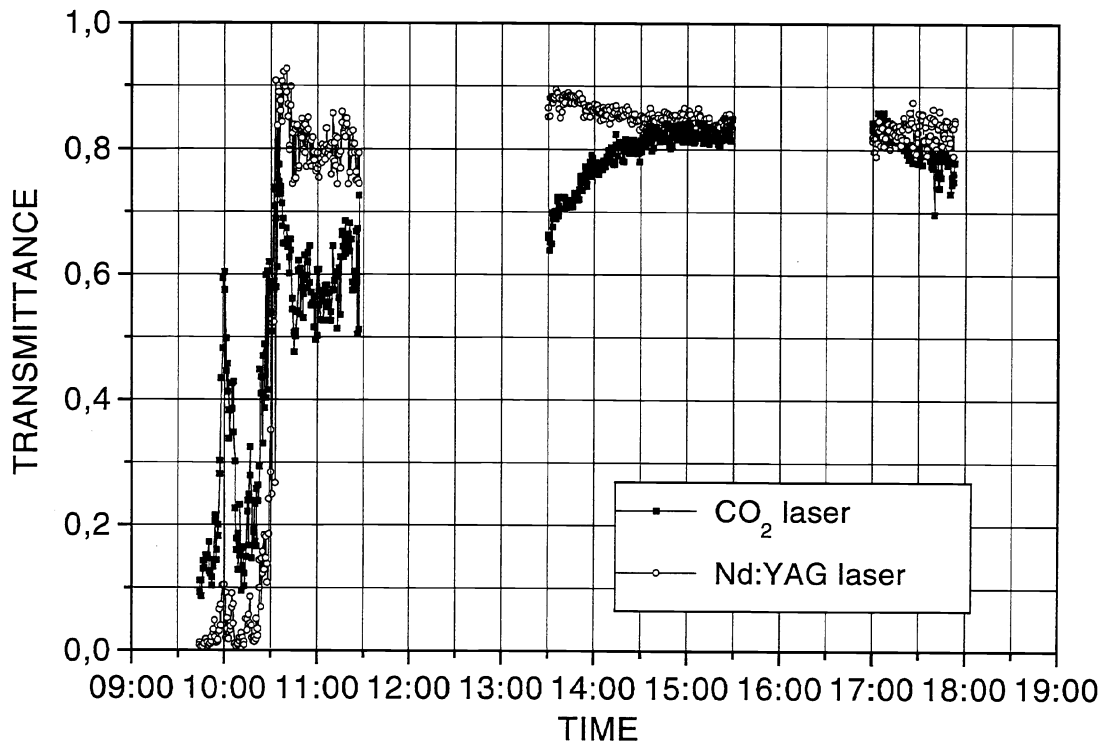
Figure 2: Diurnal variations of measured transmittance for CO_2 and Nd:YAG laser radiation during the event of 13 October 1992.

varies between 0.09 and 0.6 and $\tau(YAG)$ between 0.05 and about 0.2. The cloud finally dissipated at about 10h30 and the conditions afterwards remained clear with a slight haze layer above the valley. The transmittance values increased to approximately 0.8 in the case of the Nd:YAG laser and 0.7 for the CO_2 laser. A few minutes later, as the mountain shadow receded, the sun began to shine directly onto the very wet vegetation on the valley floor causing water evaporation. An increase of the absolute humidity from 5.5 g/m^3 at 10h30 to 6.75 g/m^3 at 11h30 was measured by the meteorological station at the valley site. This effect explains the decrease of the atmospheric transmittance for the CO_2 laser radiation from about $\tau = 0.7$ to $\tau < 0.6$. At 10h30 a group of IFU (Garmisch -Partenkirchen, Germany) launched a radio sonde to measure the atmospheric profiles of relative humidity, temperature, pressure, etc. These meteorological data were used as input parameters in the transmission code FASCOD3 to calculate the molecular transmittance and the molecular extinction coefficient for the layered atmosphere along the slant optical path from the valley site up to the summit, i.e. the transmissometer path. The molecular transmittance was calculated to be 0.994 for the Nd:YAG laser radiation and 0.848 for the CO_2 laser radiation with the corresponding molecular extinction coefficients of 0.0027 km^{-1} and 0.072 km^{-1}, respectively.

During the early afternoon, after 13h30, the absolute humidity decreased which resulted in an increase of the CO_2 laser transmittance from 0.65 at 13h30 to 0.82 at 14h30. For clear atmospheric conditions, the transmittance values τ are similar for both laser wavelengths, approximately 0.80–0.82 in the case of the CO_2 laser and slightly larger values for the Nd:YAG laser, i.e. 0.85– 0.88.

In the evening, the absolute humidity increased somewhat and caused a weak drop of $\tau(CO_2)$. For the Nd:YAG laser radiation there is no significant difference in the transmittance values measured during the early afternoon
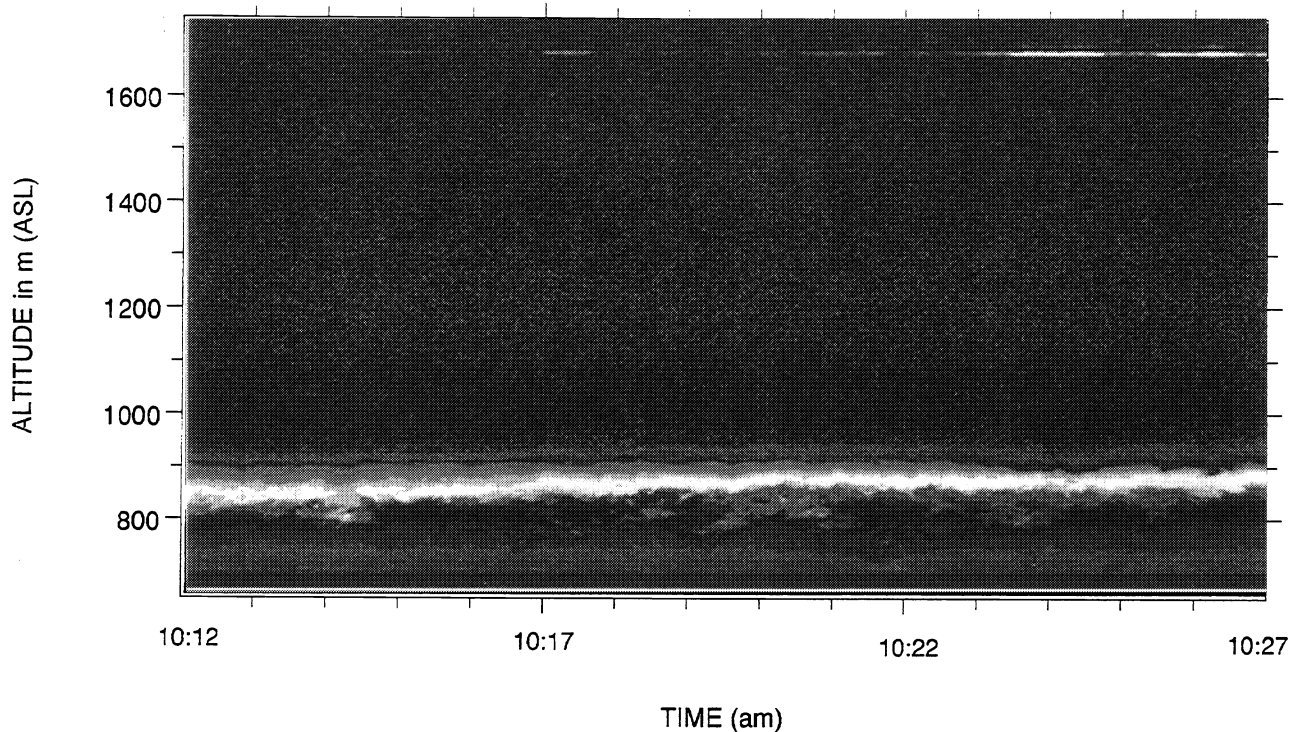
Figure 3: Grey tone representation of $\sim$ 750 slant path lidar measurements corrected for range and system parameters as functions of time. The variation of the reflected signal from the target at an altitude of $\sim$ 1750 m is caused by the transmission variations of the cloud.

and the evening period.

3.2 Reflectometer lidar versus transmissometer

On the morning of October 13 a visually homogeneous cloud layer filled the valley. Neither the mountain ridge nor the top of the mountain, where the transmissometer receiver station was located, were visible through the cloud. The cloud breadth estimated from the measured returns was between $\sim$ 150 to $\sim$ 300 m above the ground. Although the base and strength of the cloud layer can be clearly discriminated from the atmospheric returns beneath, we cannot tell whether the lidar signals ends in clear air or is completely absorbed by the cloud. However, *in situ* measurements made from a cable car that ran from the valley to the mountain top showed, in retrospect, that the atmosphere was very clear above the cloud deck and that the cloud had a thickness of about 150 m. This confirmed that the extent of the lidar signal was a true measure of the cloud thickness in that case.

During the measurements described above, the question arose as to whether it was possible to penetrate the cloud with the lidar. To verify this, the lidar was pointed at a rocky spot near the top of the mountain ridge; the angular coordinates and range to the spot ($\sim$2200 m) were determined on previous clear days. Individual measurements did not show a target return but the co-addition of successive measurements produced a good discrimination of a target signal from the regular noise pattern. In order to measure cloud transmission as a function of time, the lidar was kept pointing in that direction for more than one hour. A grey tone representation of these lidar returns, corrected for geometrical attenuation and system parameters, is reproduced in Fig. 3; the target returns are clearly shown as a line of variable intensity at the fixed altitude of $\sim$ 1750 m. The variations
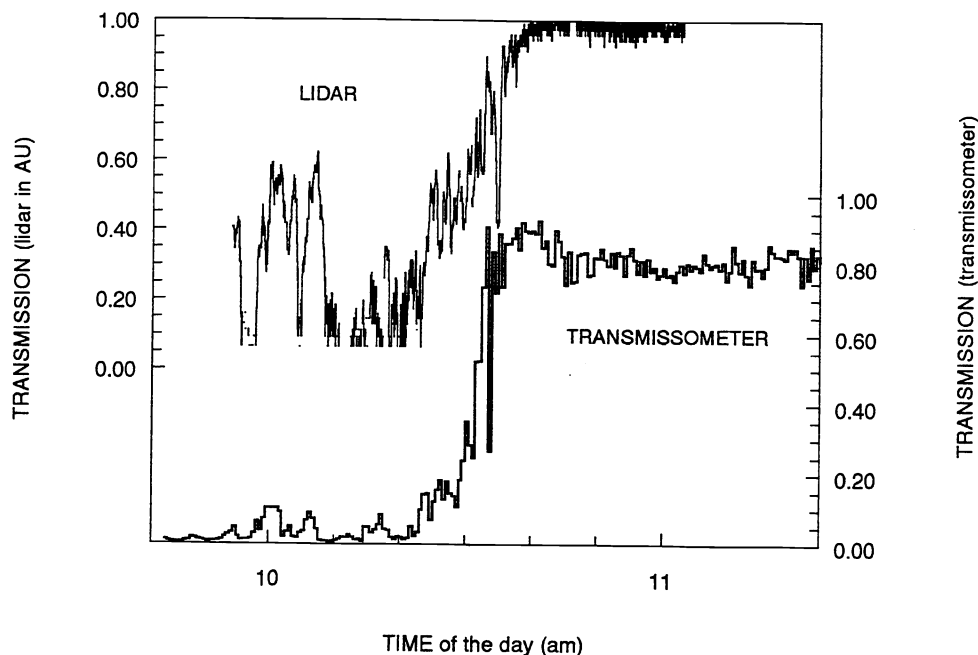
Figure 4: Comparison of time plots of transmissometer (Lower curve) and lidar-derived (Upper curve) 1.064-μm transmittances through the cloud layer of 13 October 1992 in the case of the SMAL lidar operated in the reflectometer mode.

in the target reflected signal are caused by variations in cloud transmission. Because the system parameters were kept constant during the measurements, the target reflection is a measure of the cloud transmittance. These values are shown in Fig. 4. Between 09h50 and 10h20, there are strong fluctuations in transmittance. After about 10h20, the sun rose above the top of the mountain and illuminated the cloud from the top. From that time on, the cloud dissipated very quickly and the transmission increased. The lidar data were processed in such a way that the mean noise level of the pre-trigger samples of the signal waveform was defined as the baseline whereas the maximum reflected signal was defined as a transmittance of 0.9 relative units. No attempts were made to do an absolute calibration. The differences between the transmissometer and lidar data are mainly caused by the separation between the optical axes of the two sensors.

3.3 MFOV lidar solutions versus transmissometer

Figures 5 and 6 compare the time plots of the transmittance of the cloud layer of October 13 derived from the inversion of the MFOV lidar data to the transmissometer measurements at 1.064 μm and 10.59 μm, respectively. This is the same cloud episode as used in Figs. 3-4. The transmissometer data are extracted from Fig. 2. The lidar results are the solutions of the single pulse returns recorded at a rate of 0.1 Hz and the transmissometer values are 15-s averages alternately measured at 1.064 μm and 10.59 μm. The extinction profiles necessary to calculate the lidar-derived transmittances of Figs. 5 and 6 are extrapolated from the inversion solutions for α_s and r_e, i.e. the scattering coefficient at the lidar wavelength and the effective droplet radius. The latter solutions are used to determine the parameters at each range z of the assumed gamma function for the droplet size distribution from where the extinction coefficients at 1.064 μm and 10.59 μm can be evaluated by straightforward Mie calculations.
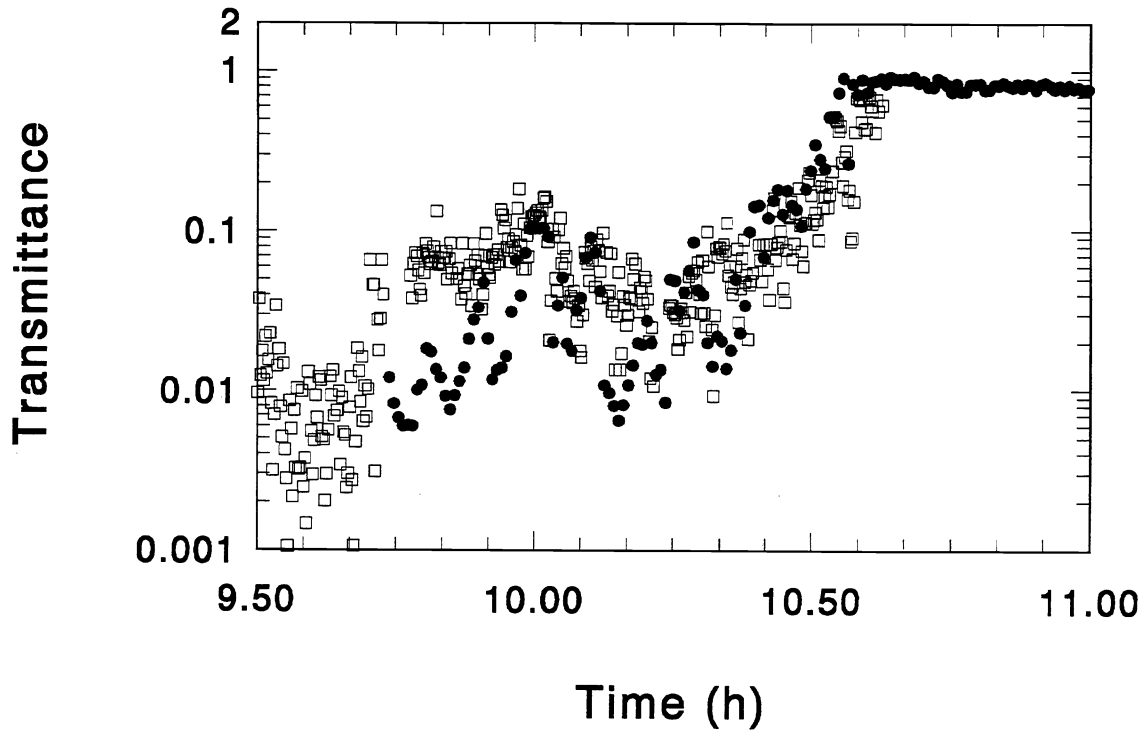
Figure 5: Comparison of time plots of transmissometer (solid disks) and lidar-derived (open squares) 1.064-μm transmittances through the cloud layer of 13 October 1992 in the case of the MFOV lidar.
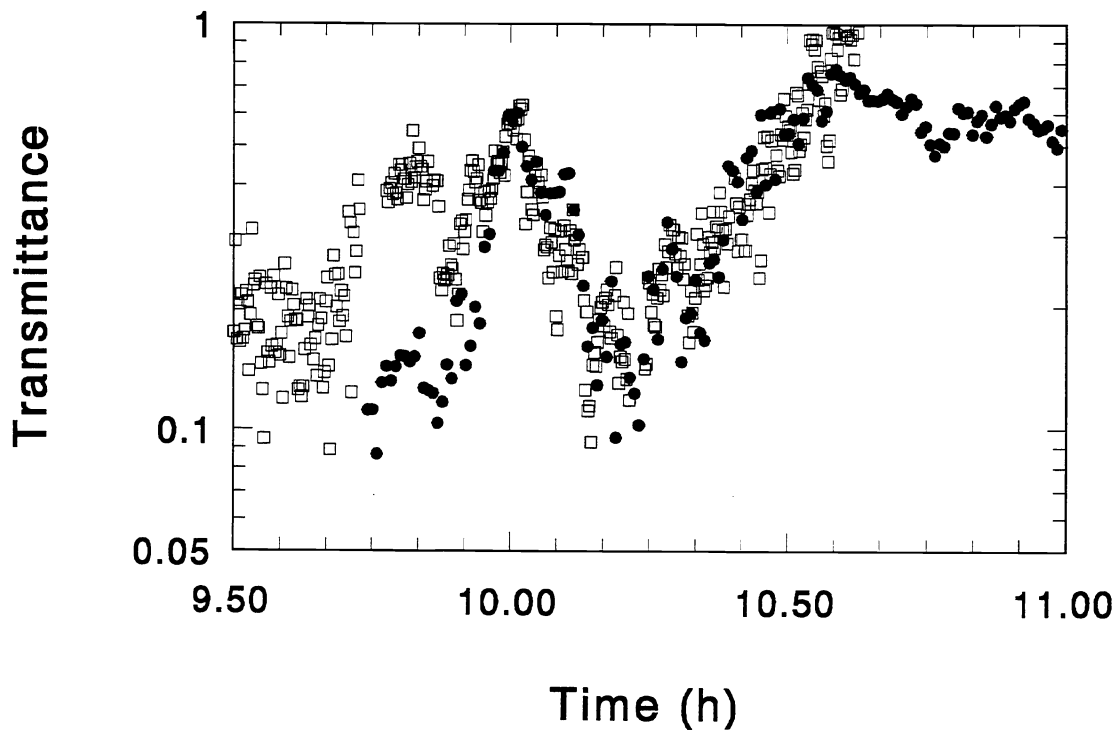

Figure 6: Comparison of time plots of transmissometer (solid disks) and lidar-derived (open squares) 10.59-μm transmittances through the cloud layer of 13 October 1992 in the case of the MFOV lidar.

The data scatter in Figs. 5 and 6 is approximately the same for both the MFOV lidar and the transmissometer indicating that it is the result of true temporal fluctuations. The fluctuations are uncorrelated because they are caused by cloud features smaller than the separation between the axes of the two instruments.

The agreement between the two measurement sets is good except for the period between 9h45 and 10h00 where the transmissometer-derived transmittance is substantially less than the lidar-derived transmittance. These differences are not due to the lidar method being limited to moderate optical thicknesses since the lidar transmittance just preceding this occurrence shows values as low as and even lower than the lowest transmissometer value of ~ 0.005. A possible explanation could be a local inhomogeneity in the size range of a few tens of meters, i.e. comparable with the separation between the lidar and transmissometer axes. Figure 4 indicates similar differences around 10h00 in the case of the SMAL lidar which was located 20-40 m from both the transmissometer and the MFOV lidar. After 10h00, the comparison shows reasonable agreement over a wide range of optical thicknesses resulting from a short-lived strengthening followed by a complete dissipation of the cloud layer.

The lidar transmittance at 1.064 μm is very nearly the integral of the solution for the scattering coefficient at the lidar wavelength because of the small difference in wavelength and the negligible absorption by water droplets. However, the transmittance at 10.59 μm depends strongly on the extrapolation method, i.e. on both solutions for the scattering coefficient and the effective droplet size. Hence, the good agreement observed in Figs. 5 and 6 is a strong indication of the validity of the solutions for both the scattering coefficient and the droplet size. This is an important result since the possibility of obtaining the effective droplet size, and hence an estimation of the extinction coefficients at other wavelengths, is a major advantage of the proposed multiple scattering method.

4 CONCLUSION

The paper compares the transmittance derived from two different lidar instruments and solution methods with calibrated transmissometer measurements over an inhomogeneous slant path through a cloud layer. In the first lidar technique, the cloud transmittance is estimated from the signal reflected off a natural target above the cloud. The second lidar had an MFOV receiver to resolve the field-of-view dependence of the multiple scattering contributions. The inversion method described in Ref. [18] is used to calculate the scattering coefficient and effective droplet radius from these data. Despite unavoidable differences resulting from the spatial separation of a few tens of meters between the lidars and the transmissometer, Figs. 4-6 show good correlation between the lidar-derived solutions and the transmissometer data. The precision is probably better than illustrated in the graphs where much of the data spread is caused by natural cloud fluctuations. In summary, the experiment validates through independent transmissometer measurements two different lidar inversion techniques and shows good correlation between the lidar solutions themselves.

The MFOV technique provides the simultaneous determination of the scattering coefficient α_s and effective droplet radius r_e. Subject to an assumption on the form of the droplet size distribution, the knowledge of both α_s and r_e allows extrapolation to extinction coefficients at other wavelengths of interest. The 1.064-μm and 10.59-μm cloud transmittances obtained in this manner correlate well with the laser transmissometer data. Hence, the comparisons of this paper also confirm the wavelength-extrapolation potential of the MFOV technique.

5 ACKNOWLEDGMENTS

successful experiment. We gratefully acknowledge the help and support of the whole team from the planning stage to the final data analysis.

6   REFERENCES

[1] J.D. Klett, "Stable analytical inversion solution for processing lidar returns," Appl. Opt. **20**, 211-220 (1981).

[2] J.D. Klett, "Lidar inversion with variable backscatter/extinction ratios," Appl. Opt. **24**, 1638-1643 (1985).

[3] G.J. Kunz, "Vertical atmospheric profiles measured with lidar," Appl. Opt. **22**, 1955-1957 (1983).

[4] J.A. Ferguson and D.H. Stephens, "Algorithm for inverting lidar returns," Appl. Opt. **22**, 3673-3675 (1983).

[5] F.G. Fernald, "Analysis of atmospheric lidar obsevations: some comments," Appl. Opt. **23**, 652-653 (1984).

[6] J.M. Mulders, "Algorithm for inverting lidar returns: comment," Appl. Opt. **23**, 2855-2856 (1984).

[7] G.J. Kunz, "Bipath method as a way to measure the spatial backscatter and extinction coefficients with lidar," Appl. Opt. **26**, 794-795, (1987).

[8] H.G. Hughes and M.R. Paulson, " Double-ended lidar technique for aerosol studies," Appl. Opt. **27**, 2273-2278 (1988).

[9] H.G. Hughes, J.A. Ferguson and D.H. Stephens, " Sensitivity of a lidar inversion algorithm to parameters relating atmospheric backscatter and extinction," Appl. Opt. **24**, 1609-1613 (1985).

[10] L.R. Bissonnette, " Sensitivity analysis of lidar inversion algorithms," Appl. Opt. **25**, 2122-2125 (1986).

[11] V.A. Kovalev, "Lidar measurements of the vertical aerosol extinction profiles with range-dependent backscatter-to-extinction ratios," Appl. Opt. **32**, 6053-6065 (1993).

[12] M. Matsumoto and N. Takeuchi, "Effects of misestimated far-end boundary values on two common lidar inversion solutions," Appl. Opt. **33**, 6451-6456 (1994).

[13] V.A. Kovalev and H. Moosmüller, "Distortion of particulate extinction profiles measured with lidar in a two-component atmosphere," Appl. Opt. **33**, 6499-6507 (1994)

[14] G.J. Kunz and G. de Leeuw, "Inversion of lidar signals with the slope method," Appl. Opt. **32**, 3249-3256 (1993)

[15] S.T. Shipley, D.H. Tracy, E.W. Eloranta, J.T. Stroga, F.L. Roesler, and J.A. Weinman, "High spectral resolution lidar to measure optical scattering properties of atmospheric aerosols. 1: Theory and instrumentation," Appl. Opt. bf 22, 3716-3724 (1983)

[16] P. Piironen and E.W. Eloranta, "Demonstration of an iodine absorption filter based high spectral resolution lidar," Optics Letters **19**, 234 (1994)

[17] A. Ansmann, U. Wandinger, M. Riebesell, C. Weitkamp, and W. Michaelis, "Independent measurement of extinction and backscatter profiles in cirrus clouds by using a combined Raman elastic-backscatter lidar," Appl. Opt. **31**, 7113-7131 (1992)

[18] L.R. Bissonnette and D.L. Hutt, "Multiply scattered aerosol lidar returns: inversion method and comparison with *in situ* measurements," Appl. Opt. **34**, 6959-6975 (1995)

[19] G.J. Kunz,"A high repetition rate lidar," TNO Physics and Electronics Laboratory, Report FEL-90-A352 (1991)

[20] ANSI Z -136.2, *For the safe use of lidars*, The Laser Institute of America, 12424 Research Parkway, Orlando, FL 32826 (1986)

[21] G.J. Kunz,"An experimental study on wind measurements with a Mie lidar," Fifth International Conference on Laser Anemometry, Advances and Applications, SPIE Vol. 2052-45, Veldhoven, The Netherlands, August 1993

[22] G.J. Kunz, "Field test of a lidar wind profiler," European Symposium on Optics for Environmental and Public Safety, SPIE Vol. 2506-20, Munich, Germany, June 1995

[23] G.J. Kunz, "Time resolved multiple-scattering," European Symposium on Optics for Environmental and Public Safety, SPIE Vol. 2506-73, Munich, Germany, June 1995

[24] L.R. Bissonnette and D.L. Hutt, "Multiple scattering lidar," Appl. Opt. **29**, 5045-5046 (1990).

[25] L.R. Bissonnette, "Multiple Scattering Technique (MUST) Lidar," U.S. Patent 5,239,352 issued Aug. 24, 1993.

[26] D.L. Hutt, L.R. Bissonnette and L. Durand, "Multiple field of view lidar returns from atmospheric aerosols," Appl. Opt. **33**, 2338-2348 (1994).